Optimal Design of Laser Surgery for Cancer Treatment Through Nanoparticle-Mediated Hyperthermia Therapy

Y. Feng[*], M. N. Rylander[**], J. Bass[*], J.T. Oden[*] and K. Diller[**]

[*]Institute for Computational Engineering and Sciences, University of Texas, Austin, USA,
{feng, bass, oden}@ices.utexas.edu
[**]Bioengineering Department, University of Texas, Austin, TX, USA,
{n.forney, kdiller}@mail.utexas.edu

ABSTRACT

Laser therapy is a minimally invasive alternative to surgical resection, but its use is limited due to the lack of specific heating due to the rate of thermal diffusion in the tissue. Nanoparticles, Nanoshells in particular, can act as intense infrared absorbers allowing enhanced thermal deposition of laser energy into tissue enabling improving the ability to damage larger tissue volumes with lower thermal doses. To design optimal nanoparticles mediated ablation therapies, an accurate understanding of the thermal distributions associated with nanoshell inclusion is essential. We present a highly accurate adaptive finite element tumor model capable of predicting the temperature and cell damage distribution due to laser heating in prostate tumor with and without inclusion of nanoshells. This model can enable optimized treatment planning based on predicted tissue response to therapy due to increased absorption from nanoshell inclusion.

Keywords: laser therapy, nanoshell, cell damage, prostate cancer, finite element modeling

1 INTRODUCTION

Cancer has become one of the leading causes of death in the United States [1]. The treatment by traditional surgical resection procedures are usually a physician's choice for removal of well-defined, primary tumors in non-vital tissue regions, however, these techniques are extremely invasive and are associated with high morbidity. In contrast, laser surgery is minimally invasive and simple to perform potentially decreasing complications and minimizing hospitalization. Laser therapies provide a lethal dose of heat to the desired site while minimizing damage to surrounding tissue. In particular, laser-induced hyperthermia therapies promise effective treatment of small, poorly-defined metastases or other tumors embedded within vital regions. The efficacy of laser therapies is limited by the lack of specificity of the heating which is dependent on the diffusion of the thermal gradient from the probe to the desired location. The dependency on diffusion requires extended heating times for large tumor volumes resulting in poorly defined damage boundaries. Therefore, large or nonuniformly-shaped tumors are not effectively treated with laser therapy.

Recent development of nanoparticle technology and its application in hyperthermia therapies enable more selective heating and lower thermal doses to be employed to achieve more precise control of the thermal energy delivered to the tumor region. This results in more effective tumor eradication and minimal destruction of surrounding healthy tissue. In this study, we consider a special class of nanoparticles called nanoshells, which can act as intense infrared absorbers increasing the thermal deposition of laser energy into the tumor. Nanoshells consist of a concentric spherical dielectric core and a thin metal coating shell with a total diameter in the 60 nm to 100 nm range, to be used as mediated agents to control the temperature field. Nanoshells possess a highly tunable plasmon resonance which determines the particle's scattering and absorbing properties. The plasmon resonance and in turn the nanoshell's optical properties can be tuned across a broad range of the spectrum from the UV to the infrared by controlling the relative thickness of the core and shell layers of the nanoshell [2,3]. In this study we confined our interest to nanoshells that are intense near-infrared absorbers in treatment of prostate cancer using laser hyperthermia therapy.

2 MATHEMATICAL MODELS

The optimal design of laser surgical protocols with nanoshell-mediated hyperthmia therapy involves reliable modeling of bioheat transfer, cell damage, effective absorption coefficient, optimization of laser source, adaptive numerical solution scheme, and quantification and control of simulation errors. In the following subsections, we briefly describe the models of choice in our study.

2.1 Bioheat Transfer Model

The mathematical representation of the temperature distribution in the tissue incorporates both the Pennes' bio-heat equation for the thermal effects of local blood perfusion and an expression for laser energy as a thermal source. We consider a laser heating source positioned inside the tumor. Let D be abounded domain (tumor region) in $\mathbb{R}^3$ with Γ denoting Lipschitz continuous boundary.

The Penne's Equation (1) is the governing equation for temperature distribution [4].

$$\rho c \frac{\partial T}{\partial t} = \nabla\left(k \nabla T\right) + \omega_b c_b (T_a - T) + Q \qquad \text{in} \qquad D \tag{1}$$

where

$$Q = \mu_{atot}\Phi = 3P\mu_{atot}\mu_{tr} \exp\left[-\mu_{eff}\left(R - r\right)\right] / 4\pi R^3$$

is the rate of absorbed laser energy per unit volume distributed within the tissue, and ρ, c, and k are the density, specific heat and thermal conductivity of the tissue, respectively. The blood perfusion rate, specific heat of blood, arterial blood temperature, and fluence are defined respectively as ω_b, c_b T_a, and Φ, respectively. The notions μ_{atot}, μ_{tr}, and μ_{eff} represent total absorption, transport attenuation, and effective irradiation coefficients. The portion of the boundary on which the temperature $\hat{T}$ is prescribed is denoted as Γ_T, and the portion on which the heat flux $\hat{q}$ is prescribed is denoted as Γ_N, where $\Gamma_T \bigcup \Gamma_N = \Gamma$, where Γ is the boundary of the tumor.

2.2 Computational Model

To proceed with finite element discretization, we define the functional space of admissible functions $\boldsymbol{V}$ as $V = \{v \in (H^1(D))^3; v = 0 \text{ on } \Gamma_T\}$, where $H^1\left(D\right)$ is the Sobolev space of functions having distributional derivatives of order one in $L^2\left(D\right)$. Furthermore, we introduce θ-family of approximations for integrating the solution forward in time. Then, the weak formulation of Equation (1) can be characterized by the following bilinear form: Given T^0, find T^{n+1} (n=0, 1, 2, 3, ……) such that

$$B(T^{n+1}, v) = B(T^n, v) + F(v) \qquad \forall\, v \in V \tag{2}$$

where

$$B(T^{n+1}, v) = \int_D \rho c (T^{n+1}/\Delta t)\, v\, dx + \int_D k\theta \nabla T^{n+1} \bullet \nabla v\, dx + \int_D c_b \omega_b (1-\theta) T^{n+1} v\, dx + \frac{1}{\varepsilon}\int_{\Gamma_T} T^{n+1} v\, ds$$

$$B(T^n, v) = \int_D \rho c (T^n/\Delta t) v\, dx + \int_D k(1-\theta)\nabla T^{n+1} \bullet \nabla v\, dx + \int_D c_b \omega_b (1-\theta) T^n v\, dx + \frac{1}{\varepsilon}\int_{\Gamma_T} \hat{T}\, v\, ds - \int_{\Gamma_T} \hat{q}\, v\, ds$$

and $F(v) = \int_D (Q - c_b \omega_b T_a) v\, dx$

This computational model is implemented on the platform of ProPHLEX® and allows specification of the thermal distribution during laser heating and study of the sensitivity of the thermal behavior to manipulation of individual source parameters. It also permits specification of equations and boundary conditions, irregular geometrical domain, optimization of the finite element mesh, visualization of the temperature, cell damage throughout the tissue, and optimization of the parameter analysis to identify target irradiation parameter values.

Prostate cancer cells inoculated in the backs of SCID mice form hemispherical shaped tumors. For the sake of computational efficiency, the quarter sphere tumor model was generated to take advantage of the symmetry for an idealized tumor model of a sphere. The boundary conditions are defined by both Direchlet and Neumann types depending on the surfaces exposed to heating. Using *a posteriori* error estimation as a guide, this method is capable of delivering exponential convergence by minimizing numerical error to specified precision.

A hexahedron 3D finite element mesh was initially defined by dividing the prostate tumor into distinct incremental volumes via the meshing operations. This model integrates both temperature and cell damage within one computational path.

2.3 Impact of Nanoshell Injection

When the tunable nanoshells are injected in the tumor region, they will significantly affect the total absorption and scattering coefficients, which in turn will alter the thermal distribution due to elevated Q. More importantly, the tunable nature of nanoshells provides more control parameters such as nanoshell's optical properties and volumetric fraction, in addition to laser power, frequency and location of applicator. The total absorption and scattering coefficient due to nanoshell inclusion can be represented as

$$\mu_{atot} = \mu_{at} + \mu_{an}, \quad \mu_{stot} = \mu_{st} + \mu_{sn} \tag{3}$$

where μ_{atot} and μ_{stot} are the total absorption and scattering coefficients due to tumor and nanoshell, where μ_{at} and μ_{st} are the absorption and scattering coefficients due to the tissue, and μ_{an} and μ_{stn} are the absorption and scattering coefficients for the nanoshells [5]. The absorption and scattering coefficients for prostate tumor measured at a wavelength of 810 nm were .046 cm^{-1} and 14.74 cm^{-1} [6]. Nanoshells with a 55 nm silica core radius and 10 nm thick gold shell were employed in the model since they have a peak absorption in the NIR [3]. A Mie theory algorithm developed by [7] was utilized to calculate the absorption and scattering cross section for these nanoshells at a wavelength of 810 nm. Then the nanoshell absorption and scattering coefficient can be calculated according to the following equations

$$\mu_{an} = 3\varphi\sigma_a / 4\pi a^3 \,,\ \mu_{sn} = 3\varphi\sigma_s / 4\pi a^3 \qquad (4)$$

where φ is the volume fraction of the particles relative to the total volume, σ_a and σ_s represent the absorption and scattering cross section respectively, and a represents the nanoshell radius [8]. The absorption and scattering coefficient due to nanoshells was .311 cm^{-1} and .2035 cm^{-1}.

The other two optical coefficients necessary for calculating Q are the transport attenuation coefficient μ_{tr} and the effective irradiation coefficient $\mu_{eff,}$ which are defined as follows:

$$\mu_{tr} = (\mu_{atot} + \mu_{stot}(1-g)\,,\ \mu_{eff} = \left(3\mu_{atot}\mu_{tr}\right)^{1/2} \qquad (5)$$

where g is the anisotropy factor.

2.4 Cell Damage Model

The availability of both thermal history and cell injury data enabled determination of the constitutive parameter values for an Arrhenius damage model:

$$\Omega(\tau) = \ln\left(C_0/C_\tau\right) = A\int_0^\tau \exp\left[-{}^{E_a}\!/_{\Re T(t)}\right]dt \qquad (9)$$

where Ω is defined as the logarithm of the ratio of initial concentration of healthy cells, C_0, to the fraction of healthy cells, $C\tau$, τ is stress duration, A is a scaling factor, *Ea* ($Jmol^{-1}$) is injury process activation energy, $\Re$ ($Jmol^{-1}K^{-1}$) is the universal gas constant, and T (^oK) is instantaneous absolute temperature of the cells during stress, which is a function of time, t (sec). The cell viability values for PC3 cells 72 hours following hyperthermia were used to determine the damage parameters employed in the Arrhenius damage model. The Arrhenius damage integral was fit to the cell injury data to characterize the response to thermal stress temperature and duration. At each temperature the threshold time τ was determined for Ω=1 for which $C\tau$ = 1/e of C_0. For isothermal stress conditions, when Ω=1 the damage equation simplifies to the logarithmic form,

$$\ln(\tau) = \left[\left({}^{E_a}\!/_{\Re}\right)\left({}^{1}\!/_{T}\right)\right] - \ln(A) \qquad (10)$$

The thermal damage kinetic coefficients of A and E_a were determined from the intercept and slope respectively of the best-fit linear function to fit the experimental data. An optimization model was then applied to refine the values of E_a and A to achieve a better match between the injury model and the experimental data.

The Arrhenius damage model described above was integrated in ProPhlex® code. The finite element model provides a predictive tool for the thermal distribution and cell damage, which is capable of assisting in the design of optimal hyperthermia protocols.

3 NUMERICAL RESULTS

Numerous simulations were conducted to investigate the effects of inclusion of nanoshells on the temperature and damage distribution. Figure 1 and 2 the temperature and damage in the tumor for both tissue alone and uniform nanoshell distribution.

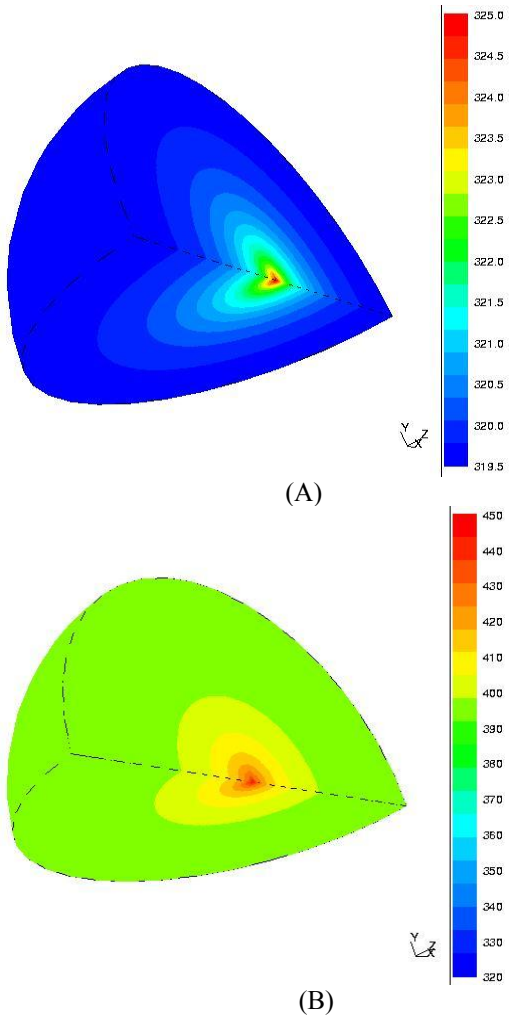

Figure 1: Temperature distribution for laser power=0.5 W for (A) tumor only and (B) with nanoshell injection.

Figure 1A, 1B, 2A, and 2B compare the temperature and damage induced by a laser power of 0.5 W, wavelength of 810 nm, and heating duration of 3 minutes for tumor with and without nanoshell injection. Enhanced thermal deposition due to injection of nanoshells caused a dramatic increase in the temperature and damage for the tumor with nanoshell injection as compared to tumor alone. Minimal damage occurred in the tumor without nanoshells whereas the entire tumor was severely injured in the tumor with

nanoshell injection. Figure 2C demonstrates how nanoshell injection decreases the requisite power from 0.5 W to 0.075 W to create similar damage profile to tumor alone depicted in Figure 2A. Table 1 summarizes the drastic difference in temperature and cell damage distribution with nanoshell injection.

Laser Power (W)	Tumor Temp. (^oK) Min/Max	Tumor Damage Min/Max	Tumor (with Nano) Temp. (^oK) Min/Max	Tumor (with Nano) Damage Min/Max
2.000	348/370	10/130		
1.000	329/340	.75/3.75		
0.500	320/325	0.1/0.6	390/405	>1000
0.100			326/337	0.6/2.4
0.075			322/330	0.2/1.0

Table 1: Various thermal doses for both tumor and tumor with nanoshell injection.

4 CONCLUSIONS

We developed an adaptive finite element tumor model capable of predicting the temperature and damage distribution due to laser heating in prostate tumor with and without inclusion of nanoshells by incorporating changes in the absorption and scattering effects. Nanoshell-mediated laser therapy enhanced the energy deposition in the tumor increasing tissue damage and reduced the requisite power necessary for tumor destruction. Using this model, optimal hyperthermia protocols can be obtained with respect to both temperature and cell damage distribution. With maturity of nano-technology such as nanoshell injection and reliable computational model, the outcome of laser surgery for cancer treatment will become more controllable and predictable.

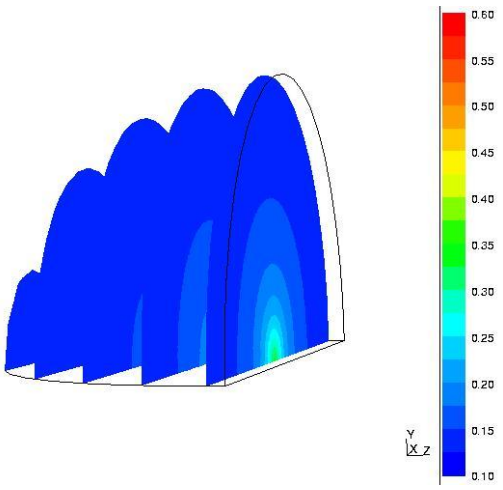

(A)

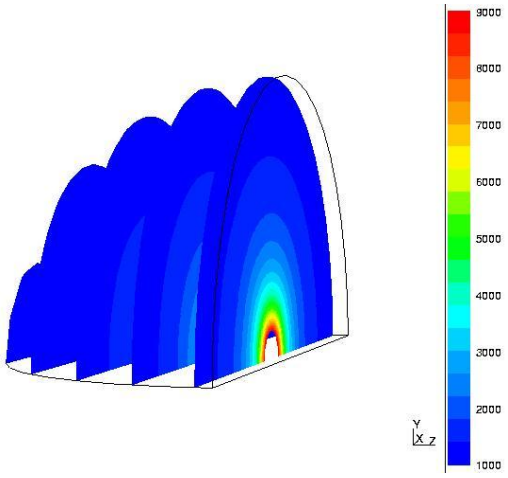

(B)

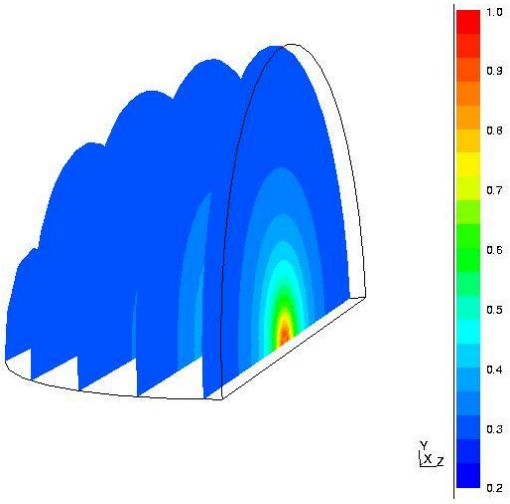

(C)

Figure 2: Damage distribution for laser power=0.5 W for A) tumor only and B) with nanoshell injection and C) laser power=0.075 W with nanoshell injection.

REFERENCES

[1] http://www.cancer.org

[2] Hirsch, L. R, Stafford, and R. J., Bankson, J. A., et al. PNAS, 100, 13549-13554, 2003.

[3] Oldenburg, S. J., Jackson, J. B., Westcott, S. L., and Halas, N. J., Appl. Phys. Lett. 75, 2897-2899, 1999.

[4] Pennes, H.H., J. Appl. Physiol., 1, 93-122, 1948.

[5] Welch and van Gemert, "Optical-Thermal Response of Laser-Irradiated Tissue," Plenum Press, 1995.

[6] Anvari, B., Rastegar, S., and Motamedi, M., IEEE Transactions on Biomedical Engineering, 14, 1994.

[7]. Travis, K. "Optical scattering from nanoparticle aggregates," Master's thesis, 2004.

[8] Liu, H., Beauvoit, B., Kimura, M., and Chance, B., Journal of Biomedical Optics, 1, 200-211, 1996.